Adaptive Level Set with region analysis via Mask R-CNN: A comparison against classical methods.

Virgínia X. Nunes[†], Aldísio G. Medeiros[*†], Francisco H. S. Silva[†], Gabriel M. Bezerra[†], Pedro P. R. Filho[*†]

[*] Federal University of Ceará (UFC), Fortaleza, Ceará, Brazil,
[†] Laboratório de Processamento de Imagens, Sinais e Computação Aplicada (LAPISCO), Federal Institute of Ceará, Fortaleza, CE
Email: {virginia.nunes, aldisio.medeiros, herculessilva, gabrielmaia}@lapisco.ifce.edu.br, pedrosarf@ifce.edu.br

***Abstract*—The World Health Organization (WHO) registered around 3 million deaths caused by Chronic Obstructive Pulmonary Disease (COPD), representing 5% of all deaths registered in 2015. Computed tomography (CT) is among the main exam for clinical diagnosis of lung diseases. However, the first challenge experienced by the radiology specialist is to define the region of interest. Thus, the identification of diseases using systems of computer-aided diagnosis (CAD) medical via image processing techniques offers more accuracy and agility for diagnosis. In this paper, we propose a new automatic segmentation of lungs in CT images. Our method uses a deep learning technique called Mask Region-Based Convolutional Neural Network (Mask R-CNN), combined with an adaptive active contour method called Fast Morphological Geodesic Active Contour (FGAC). The proposed method was evaluated with 72 lung images, consisting of 24 images of healthy volunteers and 48 of unhealthy patients. Our approach achieved promising results with Accuracy of 98.93%, Matthews Correlation Coefficient of 95.84%, Hausdorff Distance of 5.48, DICE of 96.47%, and Jaccard of 93.24%. Thus, our method surpasses a recent classic approach that also uses FGAC as a segmentation method.**

***Index Terms*—FGAC, Lung Image Segmentation, Mask R-CNN, Artificial Intelligence**

I. Introduction

The lung is one of the organs most commonly affected by diseases worldwide. Chronic Obstructive Pulmonary Disease (COPD) is the leading causes of respiratory mortality globally [1], and it was the third leading cause of death in the world, according to the World Health Organization (WHO), in 2016 [1]. In addition, according to the WHO, about 3.2 million deaths were caused by COPD in 2015, and over 90% of these deaths were in low and middle-incomecountries. It is estimated that in 2020, 200 million people worldwide will be diagnosed with COPD, and many more with these undiagnosed diseases [2].

Currently, several medical areas perform diagnostic imaging. It is mainly used to allow diagnoses to be made in a less invasive way, and to assist in the accuracy of their results, being applied in the acquisition of images of lung, heart, brain, arteries, bones, among others. Among the equipment for acquiring these images, Computed Tomography (CT) stands out [3]–[7]. CT scans allow the visualization of internal organs and the monitoring of disease evolution, in addition to reducing the number of possible diagnostic errors [8]–[10].

Diagnosis by CT exam can be improved through computer-aided diagnosis (CAD) systems. For this reason, a vast number of research studies investigate the use of CAD systems in the diagnosis of pulmonary diseases [11], [12]. In this way, segmentation techniques are applied to find regions of interest from an image. In the case of medical images, it is common to use segmentation methods to demarcate organs and associate them with the study of pathologies.

Among the techniques applied to automate the task of marking pulmonary regions, we can mention Digital Image Processing (DIP) techniques, such as morphology [13], region growing [14], and watershed transform [15]. However, traditional techniques do not obtain consistent segmentation for regions with low contrast parenchyma, leading to inappropriate results when applied on CT exams [16].

Successfully recent works using Convolutional Neural Network techniques for classification, segmentation and detection of objects of interest in images have been proposed [17], [18]. However, for conducting the proper training of these deep models requires a large set of medical images and this remains a challenge medical domain [19]. Despite this, several studies using deep learning methods for automatic detection of objects of interest in medical images have been developed. For example, a type of CNN called Mask R-CNN [20] is automatic detection and classification of the tear in the knee meniscus was presented in [21]. In Medeiros et al. [22] a new approach using Mask R-CNN to automatic initialization to segmentation of left-ventricle was successfully adopted.

Active Contour Method (ACM), also known as Snakes, demonstrates to be efficient when applied to medical images, even with the presence of noise in 2D images, due to its adaptive potential [23]–[25]. This segmentation method is based on segments of lines that evolve, forming a curve in the image domain. The curve adapts according to the shape of the region around the starting point and develops within the limits of the object of interest. The evolution of the curve aims to minimize the total energy formed by energies that depend on the active contour geometry, the internal energy, and image characteristics that form the external energy [26].

978-1-7281-6926-2/20/$31.00 ©2020 IEEE

Traditionally, ACMs need an initial contour definition, in which the segmentation result can change according to the location where the contour was defined. When the starting contour is applied in regions with concavity, protrusions, or bifurcations, it can lead to unexpected results [16]. In the case of CT scans of the lung, a possible treatment is to pre-process the images to enhance and standardize the texture of the lung, guiding the segmentation method to reduce noise interference.

Thus, to surpass these limitations, this work provides a new approach to lung segmentation based on a recent method called Fast Morphological Geodesic Active Contour (FGAC), proposed by Medeiros et al. [27]. Additionally, combined with FGAC, we present an automatic initialization method that detects the lungs and initializes a curve for each one. These curves resemble the edges of the region of interest, presenting impressive progress in the segmentation step. Therefore, it accelerates the convergence time of the approach. Our approach uses the recent deep learning called Mask R-CNN. Finally, we compare it with other lung segmentation methods.

This work is divided into sections. Section 2 presents a bibliographic review of the main topics related to this work. In Section 3, we present the FGAC approach to lung segmentation based on morphological geodesic active contour. In Section 4, we discuss the details of the proposed approach used as an initialization for FGAC. We present the results and discussions in the Section 5 and the conclusions in Section 6.

II. Related Works

Different segmentation methods based on ACM have been proposed in the literature. This section shows the main works, based on ACM and FGAC, used for comparison in the section of results and discussion.

Gradient Vector Flow (GVF) proposed by Xu and Jerry L [28] is based on gradient vectors for the evolution of the curve in regions with low definition edges. However, GVF has limitations when initialized at regions distant from the center of the object or in concave and invariant regions. The vector flow can be canceled because the gradient tends to zero, and the curve stops prematurely.

Vector Field Convolution (VFC) proposed by Li and Scott T [29] considers that external energy can be a convolution operation. Compared to GVF, VFC has advantages regarding computational cost, since it is reduced. Besides, it has greater robustness as to the initialization position of the curve, in addition to handling better when subjected to Gaussians and noisy images. However, when the curve initialization is inserted in an object that does not have a good contour definition, VFC goes beyond its edges, evolving the curve to edges of high intensity.

ACM Crisp proposed by Rebouças et al. [23] different from the previous methods, presents a new approach in which it considers the internal structures of the pulmonary parenchyma, such as vessels, airways, and pulmonary wall. These structures, when reproduced in the image, can generate false borders and confuse the evolution of the curve. The AMC Crisp is inspired by the density of lung tissues to establish image analysis ranges, based on Hounsfield units (HU). The method incorporates heuristics related to knowledge of the intensity ranges in HU. However, although innovative in density analysis, the method has limitations when the initial curve is established in decentralized regions and suffers from changes in topology in the image [30].

Adaptive ACM Crisp (CRAD) proposed by Rebouças et al. [30] an improvement on the Crisp [23] method, presents optimizations regarding the limitations of decentralized initializations in the region of interest. However, this method requires defining the set of categories according to the density of the tissues and the previous training of the classifier, imposing time limitations to reach a solution.

According to Barros [31] the Optimum Path Snakes (OPS) is a technique inspired by the classifier Optimum Path Forest (OPF). In this method, each point on the curve, taken as an explorer point, is able to analyze the neighborhood and determine the optimal path to evolve. Similar to CRAD, the OPS method is based on the optimization of the OPF classifier and, likewise, requires prior training of the points that represent the class prototypes.

To improve the segmentation methodology, the works using transforms as the Radial Hilbert Transform (RHT) proposed by Felix et al. [32] were also used for comparison.

A recent work proposed by Medeiros et al. [27] uses the FGAC method for lung segmentation with an automatic initialization that approximates the initial contour of the desired segmentation region. However, proposed initialization to FGAC presents high sensitivity to the calculation of the gradient present near edges of objects of interest when they are close, which leads to an unwanted segmentation. In this sense, our work presents an adaptive approach for localization of the region of interest. Our method is based on the analysis of local regions using a recent pixel classification technique, which is inspired by Convolutional Neural Networks based on region, known as Mask R-CNN.

III. Materials

This section describes the methods that substantiate this work, as well as the description of the dataset and evaluation metrics.

A. A fast segmentation via Morphological Geodesic Active Contour

Osher-Sethian [33] proposed the representation of a deformable curve C as a embedded curve in a ϕ function. The ϕ function is known as level set. Posteriorly, Caselles et al. [34] proposed the geodesic active contour as a deformable model inspired by the Osher-Sethian level set. As an evolution of Caselles et al. method, Medeiros et al. [34] proposes the Fast Morphological Geodesic Active Contour (FGAC). This image segmentation method is based on the equivalence of morphological operators with differentiable functions, proposed by Marquez-Neila et al. [35].

Unlike traditional active contours, FGAC does not depend on the parameterization of each point on the curve. The

978-1-7281-6926-2/20/$31.00 ©2020 IEEE

evolution of the C curve points is based on the deformation of the geometric shape that defines the segmentation level set. The minimization of energy functional designates the reduction of the geodesic distance. This reduction deformities geometric shape that determines the deformation of segmentation level set. The Equation 1 defines the energy functional:

$$E(C) = \int_0^{length(C)} \Omega(I)(C(s))ds \quad (1)$$

where $C(s)$ is the segmentation curve and $\Omega(I)$ detects high gradient regions in the image.

The FGAC segmentation method represents the level set as a group of pixels in a binary image. However, to identify the initial level set, FGAC presents high sensitivity to the calculation of the gradient present at the edges of objects when they are very close to each other, which leads to an unwanted segmentation.

B. Mask R-CNN

He et al. [20] proposed a method called Mask R-CNN for detection, classification, and segmentation of objects based on Region-based Convolutional Neural Network architectures, such as R-CNN [36], Fast R-CNN [37], and Faster R-CNN [38]. Two competing CNNs form the structure of the Mask R-CNN: a Region Proposal Network (RPN), used to detect and classify objects, and a Fully Convolutional Network (FCN), that has the function of generating object segmentation masks [20]. The improvement of the net result is performed using the loss function described in Equation 2,

$$L = L_{clc} + L_{bbox} + L_{mask} \quad (2)$$

where L is the total training loss, L_{clc} is the object classification loss, L_{bbox} is the object detection loss, and L_{mask} is the segmentation mask error.

C. Image acquisition

The proposed method was evaluated using a CT dataset of lung diseases, provided by Walter Cantidio University Hospital, in Fortaleza, Brazil. This dataset consists of 24 images of healthy lungs and 48 of unhealthy lungs: 24 with fibrosis and 24 with pulmonary emphysema. The same dataset was used in previous experiments, such as disease classification [39]–[41] and image segmentation [27], [42]. The exams were obtained by two different types of equipment: Toshiba Aquilion GE Medical System LightSpeed 16 and Philips Brilliance 10. Since the exams were collected by different equipment, they showed irregularities in lighting and contrast. However, all exams have a resolution of 512 x 512 pixels with 16 bits.

D. Evaluation Metrics

In order to evaluate the average generalization of the proposed initialization method combined with FGAC, we use the following evaluation metrics for segmentation: Accuracy (ACC) [43], [44], Sensitivity (Se) [43], [44], Dice Coefficient (DICE) [45], Matthews Correlation Coefficient (MCC) [46], Jaccard Index (JAC) [47] and Hausdorff Distance (HD) [48].

IV. Adaptive Level Set with region analysis via Mask R-CNN.

Previous studies on segmentation methods based on deformable models indicate that the initialization stage is a critical stage for the performance of the method. Techniques based on the image gradient, for instance, can converge early on uniform regions of the image. In this section, we present a new approach for calculating the region of interest, based on the classification of local regions. This approach involves the FGAG method adding an adaptive potential to detection of region of interest. It combines the representative potential of Mask R-CNN to detect regions of interest with the ability of FGAC to deform the segmentation curve. Thus, we call our method as R-FGAC.

In Figure 1, we show the structure of the proposed method, consisting of three main steps, which will be described in the following subsections.

A. Pre-processing

Pre-processing is a critical step for CT images since it helps in subsequent steps of segmentation. Contrast Limited Adaptive Histogram Equalization (CLAHE) has produced excellent results on medical images [49]. Several works have been done using CLAHE for image enhancement, such as [50]–[53]. As shown in Step 1 of Figure 1, the exams are pre-processed using the CLAHE filter. In this way, the regions of interest become more noticeable. The improvement with the application of this pre-processing in the images contributes to achieving better initialization results obtained by Mask R-CNN after training the model.

B. Classification

1) Augmentation: Computed tomography images, especially chest projections, present organs in shapes that vary according to the analysis plan. In this respect, it is necessary to train the model with varied samples aiming to improve the generalization potential of the classifier. In this work, the image dataset was expanded, generating samples under applications of rotation, mirroring, and translation of the original image. Figure 2 illustrates the different changes on a CT scan and their synthetic variations.

2) Mask R-CNN Training Stage: We used Mask R-CNN with Inception Resnet v2 for training, as can be seen in the overview of this models [1]. Since there were just over 270 images of the lung, we opted for pre-trained weights. The pre-trained weights on the COCO dataset [2] were used as initial

[1]https://github.com/tensorflow/models/blob/master/research/object_detection/g3doc/detection_model_zoo.md

[2]http://cocodataset.org/

978-1-7281-6926-2/20/$31.00 ©2020 IEEE

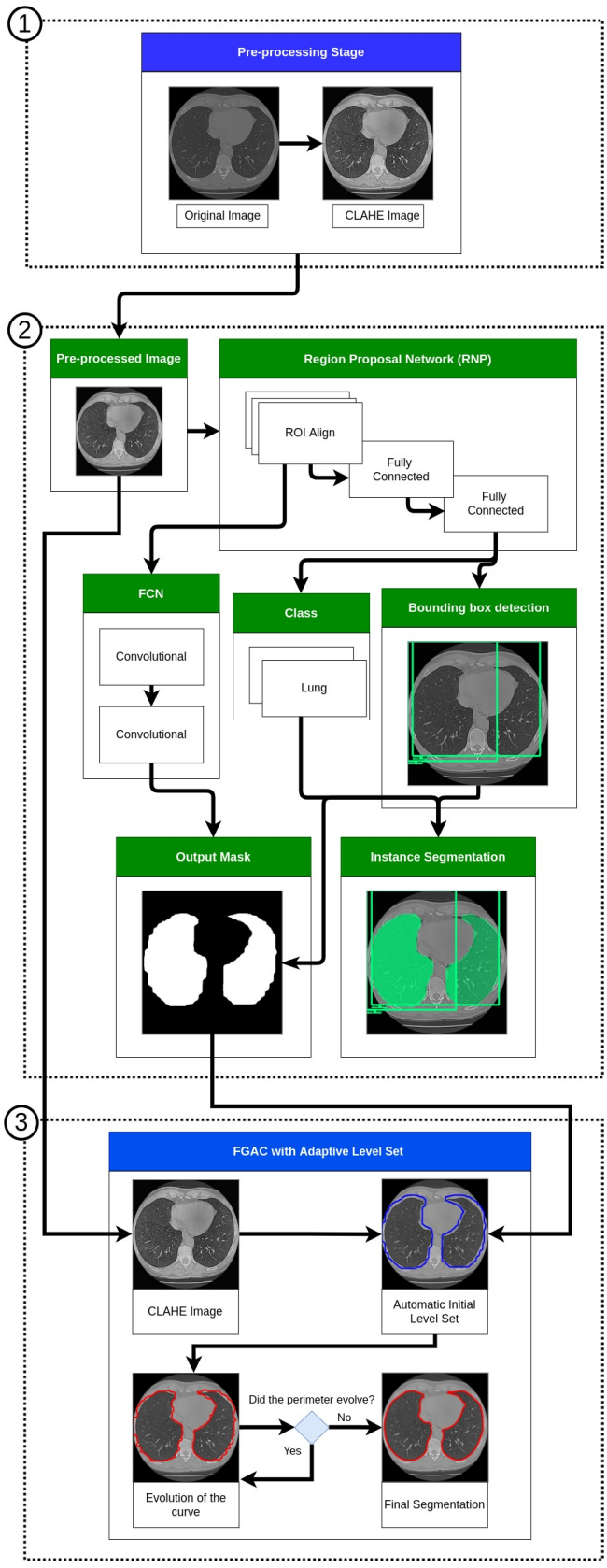

Fig. 1. Overview of the steps of proposed approach to lung segmentation via RMask-FGAC.

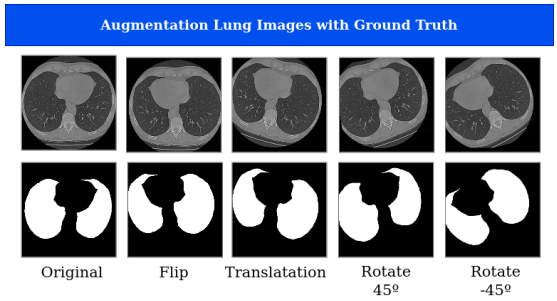

Fig. 2. Dataset regularization technique via data augmentation.

weights in training. For attribute extraction, we set the batch size to 1. Also, we established an Intersection over Union (IoU) threshold of 0.7 to filter detections with poor quality. Additionally, we assigned 0.9 to momentum without Dropout.

For conduct adequate training of the deep model for extraction representative features from the data, in the training stage, it performed 100,000 iterations over the augmented data. Initially, the learning rate was 0.003, decreasing to 0.0003 after 70,000 iterations. The total training time was 12 hours, using the augmented image set. At the end of the training, the Total Loss was uniform and below 2%.

C. Adaptive Level Set

According to the work of Medeiros et al. [27] and Rebouças Filho [54], the initialization stage presents itself as a critical step for segmentation methods based on deformable models. In this work, we propose the identification of Level Set zero as a binary component obtained by analyzing local regions and detecting candidate regions from the output of the Mask R-CNN.

After Mask R-CNN training, the model is able to detect and segment objects that were presented during its training. Step 2 of Figure 1 illustrates the processes done by Mask R-CNN, from its input to its output. Firstly, we show the pre-processed image as an input to RNP, where an ROI Align is performed to generate the input for the Fully Connected Layers and for the FCN. Then, the Fully Connected Layers perform the class and bounding box predictions, whereas the FCN is responsible for creating the segmentation masks.

The two binary components identified in Step 2 are used as an initial level set. They cover a region overlapping the thoracic concavity, thus representing a region where the lung will be contained. In this sense, these components form the initial level set that must be deformed in order to find the borders that represent the pulmonary walls.

D. FGAC with Adaptive Initialization

Finally, the last step of Figure 1 represents the initialization of the active contour R-FGAC, using the adaptive level set identified in the previous step through the Mask R-CNN. At this stage, the active contour R-FGAC initializes its segmentation curve, i.e., level set zero, and contracts the curve towards the lung walls where there is a greater incidence of

978-1-7281-6926-2/20/$31.00 ©2020 IEEE

the gradient in the image. This evolution is an iterative process and continues until the perimeter of the curve stops evolving.

V. Results and Discussion

In this section, we discuss the results of different classic approaches for locating the region of interest proposed in methods such as GVF [28], VFC [29], Crisp [23], CRAD [30], OPS [31], and original FGAC [27]. All methods were applied to the same lung samples of the dataset to a equivalent comparison. Our method is compared with the previous approaches, according to the similarity between their results and the expert segmentation.

The results are divided into three parts: quantitative indexes (Sen, ACC, and MCC), similarity indexes (HD, DICE, and JAC), and segmentation time. We use only the quantitative and similarity indices to determine the best configuration for our method. In order to compare with the other methods mentioned, we use all three types of results.

All experiments were conducted on Ubuntu 18.04 operating system with 16GB RAM, Intel Core i7 processor, and NVIDIA GeForce GTX 1660 TI GPU.

According to Medeiros et al. [27] geodesic active contour requires three parameters: σ as the Gaussian derivatives, v as the ballon force, and α as a weight factor to the gradient. As in their work, we set the α parameter to 1000. Then, we perform a grid search to find the best combination for the parameters σ and v. The search interval for σ was defined between 1 and 5 with a variation of 1, and v was defined between 0.25 and 0.50 with a variation of 0.05. Table I presents the results for the proposed combinations and the respective values for the parameters mentioned above.

The best combination values found within the determined ranges were σ equal to 3.0 and v equal to 0.25. With this combination, it is possible to obtain the best lung segmentation for this data set compared to the ground truth provided by the specialist.

Table II shows the shortest average time of execution for each method. The proposed approach achieved 4.3±0.04 seconds for the best combination of parameters. GVF had the longest time and standard deviation, with 240.00±3.05 s. FGAC had the shortest time, with only 001.85±0.50 s. The proposed method surpasses GVF, VFC, OPS Euclidian, and SISDEP, which had segmentation time of 240.00±3.05, 030.00±2.67, 008.27±2.63, 005.86±1.96, and 004.90±2.02 seconds, respectively. Our approach achieved the lowest standard deviation, indicating greater stability in the time to obtain segmentation.

Table III presents the mean values and standard deviations of the quantitative measures ACC, MCC, and Se. The configuration of the proposed R-FGAC combination that obtained the best results equaled or surpassed the average accuracy achieved by VFC, GFV, THR mod, THR multi, OPS Euclidean, SISDEP, CRISP, and the recent FGAC. The only exception was CRAD, which was 0.06 higher. Considering the MCC index, our method reached 95.84±01.90%, surpassing all methods, except for OPS Euclidian, SISDEP, and CRAD.

TABLE I
Grid Search of Gaussian derivatives (σ) and Ballon Force (ν) to find the best parameters. The best combination of the values σ and ν is highlighted in green. The results were evaluated according to Accuracy (Acc), Matthews Correlation coefficient (MCC), Sensitivity (Se), Hausdorff distance (HD), Dice coefficient (DICE), and Jaccard index (Jac).

σ	ν	ACC	MCC	Se	HD	DICE	Jac
1.0	0.25	98.81	95.33	95.00	5.63	96.02	92.41
1.0	0.30	98.82	95.42	96.33	5.66	96.11	92.57
1.0	0.35	98.81	95.45	97.46	5.67	96.14	92.62
1.0	0.40	98.79	95.39	97.91	5.70	96.10	92.52
1.0	0.45	98.77	95.36	98.24	5.66	96.07	92.48
1.0	0.50	98.74	95.30	98.45	5.66	96.02	92.38
2.0	0.25	98.91	95.76	95.33	5.48	96.40	93.11
2.0	0.30	98.90	95.74	95.5	5.47	96.38	93.08
2.0	0.35	98.87	95.64	96.32	5.50	96.31	92.94
2.0	0.40	98.85	95.65	97.79	5.54	96.32	92.93
2.0	0.45	98.83	95.60	98.25	5.47	96.27	92.84
2.0	0.50	98.82	95.59	98.48	5.49	96.26	92.82
3.0	0.25	98.93	95.84	95.46	5.48	96.47	93.24
3.0	0.30	98.92	95.84	95.52	5.45	96.46	93.23
3.0	0.40	98.91	95.57	96.20	5.47	96.41	93.12
3.0	0.45	98.86	95.67	97.57	5.46	96.34	92.98
3.0	0.50	98.85	95.69	98.28	5.40	96.35	92.99
4.0	0.25	98.92	95.83	95.43	5.45	96.46	93.22
4.0	0.30	98.92	95.83	95.43	5.45	96.46	93.22
4.0	0.35	98.91	95.81	95.42	5.47	96.44	93.21
4.0	0.40	98.92	95.81	95.48	5.45	96.44	93.20
4.0	0.45	98.92	95.79	96.08	5.51	96.43	93.16
4.0	0.50	98.87	95.69	96.28	5.52	96.36	93.01
5.0	0.25	98.91	95.76	95.31	5.54	96.39	93.11
5.0	0.30	98.91	95.76	95.31	5.54	96.39	93.11
5.0	0.35	98.91	95.76	95.31	5.54	96.39	93.11
5.0	0.40	98.89	95.75	95.39	5.53	96.38	93.09
5.0	0.45	98.91	95.75	95.36	5.53	96.39	93.09
5.0	0.50	98.90	95.73	95.96	5.58	96.37	93.06

TABLE II
Average segmentation time of the proposed method against other methods.

Methods	Average time (s)
GVF	240.00±3.05
VFC	030.00±2.67
OPS	008.27±2.63
OPS Euclidean	005.86±1.96
SISDEP	004.90±2.02
CRAD	002.00±0.16
FGAC	001.85±0.50
R-FGAC	004.3±0.04

However, the highest MCC, reached by OPS Euclidean, was only 0.3 higher. Besides, the proposed method achieved a better average time performance compared to OPS Euclidian.

Regarding the sensitivity index, our approach reached 95.46±03.64%, which was below the average of the other approaches. Unlike the other methods, we configured FGAC to perform the evolution of the curve to contract and adjust the outer edges of the lung. Due to the physiognomy of the lungs having many concavities and non-uniform regions, FGAC was not able to contract in order to adjust to very concave and narrow regions. Thus, in some exams that presented such characteristics, the final segmentation obtained remained external to these details, impairing sensitivity.

978-1-7281-6926-2/20/$31.00 ©2020 IEEE

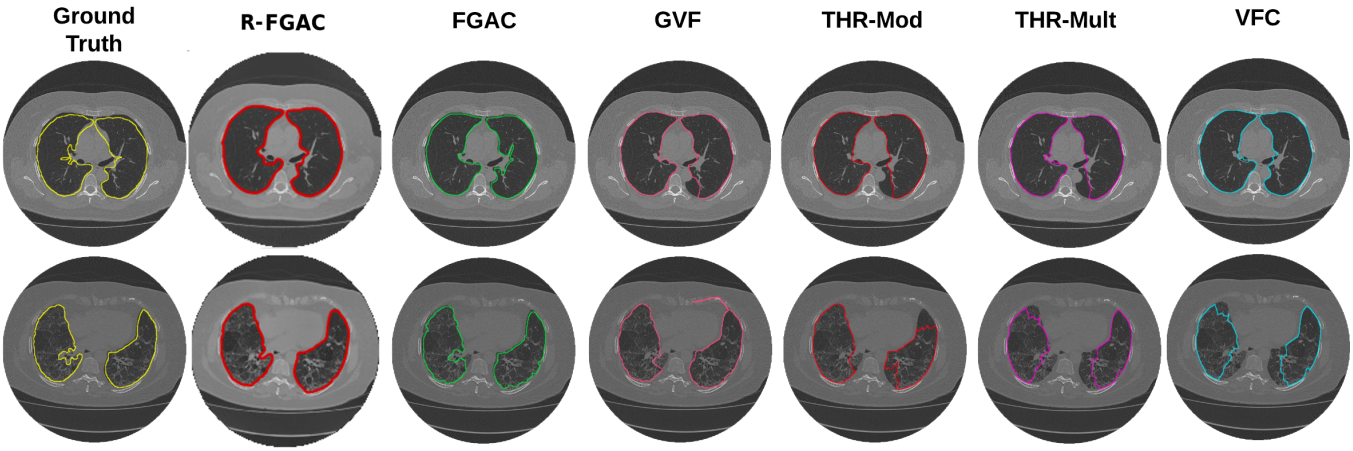

Fig. 3. Comparison between R-FGAC and the segmentation methods that obtain initializations via classic methods. The first line shows healthy lungs and highlighted segmentation. The second line shows the lungs with pulmonary fibrosis and highlighted segmentation.

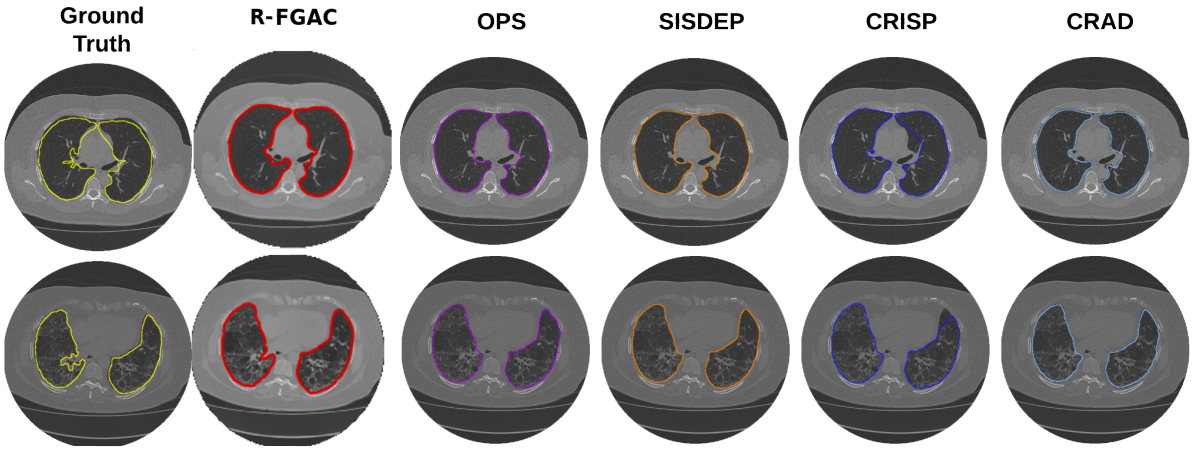

Fig. 4. Comparison between R-FGAC and the segmentation methods that obtain initializations via supervised algorithms. The first line shows healthy lungs and highlighted segmentation. The second line shows the lungs with pulmonary fibrosis and highlighted segmentation.

TABLE III
QUANTITATIVES INDEXES TO COMBINATION OF R-FGAC AGAINST OTHERS SEGMENTATION METHODS.

ACM	Quantitative indexes		Se
	Acc	MCC	
R-FGAC	98.93±00.44	95.84±01.90	95.46±03.64
FGAC	98.86±0.46	95.54±1.92	99.21±0.66
VFC	97,88±01,29	92,13±03,20	98,26±01,31
GVF	96,79±03,61	90.00±06,45	96,75±05,10
THR mod	97,56±01,63	91,34±03,09	98,22±01,28
THR multi	95,77±3,96	85,38±11,85	97,68±03,45
OPS Euclidean	98,93±0,53	96,14±1,29	99,00±0.79
SISDEP	98,89±0,52	95,87±1,13	98,99±0,65
CRISP	98,04±0,89	92,67±2,73	98,01±1,23
CRAD	98,99±0,57	96,13±1,86	99,45±0,43

For similarity indexes, Table IV presents the mean values and standard deviations of the HD, DICE, and Jaccard values. The R - FGAC reached 5.48±1.13%, 96,47±01,91%, and 93,24±03,38% for HD, DICE, and Jaccard metrics, respectively. Considering the HD index, R - FGAC had a better performance than FGAC, VFC, GVF, THR mod, THR multi, and CRISP methods. Also, the proposed method achieved results similar to OPS Euclidian, SISDEP, and CRAD, being only 0.34 below CRAD. Similarly, for DICE and Jaccard indexes, R - FGAC surpassed FGAC, VFC, GVF, THR mod, THR multi, and CRISP. The R-FGAC reached equivalent results to OPS Euclidian, SISDEP, and CRAD, regarding DICE and Jaccard indexes. For the DICE measure, for example, the results show that the biggest difference is only 0.29 between the OPS Euclidian and R - FGAC. Likewise, for the Jaccard measure, the difference between OPS Euclidian and R - FGAC is only 0.51.

For purposes of visualization and comparison of segmentation methods, Figures 3 and 4 show the final segmentation of R-FGAC, comparing it to other methods, for healthy lungs and lungs with pulmonary fibrosis.

VI. CONCLUSIONS AND FUTURE WORK

In this work, we propose a new robust technique for automatic lung segmentation in CT scans of the lung. In

978-1-7281-6926-2/20/$31.00 ©2020 IEEE

TABLE IV
SIMILARITY INDEXES TO R-FGAC AGAINST OTHERS SEGMENTATION METHODS.

ACM	Similarity Indexes		
	HD	DICE	Jaccard
R-FGAC	5.48±1.13	96,47±01,91	93,24±03,38
FGAC	5.57±1.17	96.19±1.93	92.73±3.43
VFC	6.92±1.50	93,33±2,82	87,62±4,81
GVF	7.55±2.29	91,76±4,84	85,11±7,71
THR mod	6.93±1.79	92,81±2,21	86,65±3,79
THR multi	8.23±2.91	87,29±11,18	78,82±14,43
OPS Euclidean	5,29±1,14	96,76±1,12	93,75±2,09
SISDEP	5,46±1,15	96,52±1,01	93,3±1,87
CRISP	6,33±1,32	93,73±2,7	88,31±4,56
CRAD	5,14±1,17	96,73±1,73	93,72±3,15

this approach, we combine the morphological geodesic active contour with a new adaptive initialization via deep learning technique. Our approach applied the Fast Morphological Geodesic Active Contour (FGAC) at the final output of the Mask R-CNN network.

We analyzed different studies that carried out to automatically identify and segment the lung region. Among the ones that use a classic initialization, FGAC stood out. This method achieved Accuracy of 98.86%, Matthews Correlation Coefficient (MCC) of 95.54%, Hausdorff Distance (HD) of 5.57, DICE of 96.19%, and Jaccard (Jac) of 92.73%. On the other hand, our approach combines a deep learning technique, via Mask R-CNN, with FGAC. As a result, we achieved higher metrics values, such as Accuracy of 98.93%, Matthews Correlation Coefficient of 95.84%, Hausdorff Distance of 5.48, DICE of 96.47%, and Jaccard of 93.24%.

Given that a typical CAD system for the diagnosis of pulmonary diseases consists primarily of a lung segmentation stage, the development of lung segmentation techniques is relevant. This work introduced an innovative technique for automatic lung segmentation in medical images using a recent and powerful approach to achieve more accurate and agile results. Instead of the pulmonary regions in CT scans being marked manually by an expert, our approach will support the specialist in this step, providing more efficient segmentation quality.

Thanks to the generalization power of Mask R-CNN for object segmentation, for future works, we intend to apply the technique to another set of lung data with greater volume and variability in order to improve the prediction of Adaptive Level Set with Mask R-CNN. We also intend to evaluate new deep learning techniques based on the region's classification. Finally, we also intend to evaluate these techniques in other sets of medical images, given the high power of generalization learning.

ACKNOWLEDGMENT

The authors would like to thank The Ceará State Foundation for the Support of Scientific and Technological Development (FUNCAP) for the financial support (6945087/2019). This study was financed in part by the Coordenação de Aperfeiçoamento de Pessoal de Nıvel Superior - Brasil (CAPES) - Finance Code 001". Also Pedro Pedrosa Rebouças Filho acknowledges the sponsorship from the Brazilian National Council for Research and Development (CNPq) via Grants Nos. 431709/2018-1 and 311973/2018-3.

REFERENCES

[1] J. B. Soriano, A. A. Abajobir, K. H. Abate, S. F. Abera, A. Agrawal, M. B. Ahmed, A. N. Aichour, I. Aichour, M. T. E. Aichour, K. Alam, et al., Global, regional, and national deaths, prevalence, disability-adjusted life years, and years lived with disability for chronic obstructive pulmonary disease and asthma, 1990–2015: a systematic analysis for the global burden of disease study 2015, The Lancet Respiratory Medicine 5 (9) (2017) 691–706.

[2] N. L. Ford, I. Lee, A. Tam, D. D. Sin, Micro-computed tomography imaging of a rodent model of chronic obstructive pulmonary disease (copd), in: Medical Imaging 2020: Biomedical Applications in Molecular, Structural, and Functional Imaging, Vol. 11317, International Society for Optics and Photonics, 2020, p. 113172F.

[3] G. T. Herman, Fundamentals of computerized tomography: image reconstruction from projections, Springer Science & Business Media, 2009.

[4] M. W. Vannier, Ct clinical perspective: challenges and the impact of future technology developments, in: 2009 Annual International Conference of the IEEE Engineering in Medicine and Biology Society, IEEE, 2009, pp. 1909–1912.

[5] P. L. Vidal, J. de Moura, J. Novo, M. Ortega, Cystoid fluid color map generation in optical coherence tomography images using a densely connected convolutional neural network, in: 2019 International Joint Conference on Neural Networks (IJCNN), IEEE, 2019, pp. 1–8.

[6] J. H. Alves, P. M. M. Neto, L. F. Oliveira, Extracting lungs from ct images using fully convolutional networks, in: 2018 International Joint Conference on Neural Networks (IJCNN), IEEE, 2018, pp. 1–8.

[7] R. Golan, C. Jacob, J. Denzinger, Lung nodule detection in ct images using deep convolutional neural networks, in: 2016 International Joint Conference on Neural Networks (IJCNN), IEEE, 2016, pp. 243–250.

[8] M. Muzammal, R. Talat, A. H. Sodhro, S. Pirbhulal, A multi-sensor data fusion enabled ensemble approach for medical data from body sensor networks, Information Fusion 53 (2020) 155–164.

[9] A. H. Sodhro, Y. Li, M. A. Shah, Energy-efficient adaptive transmission power control for wireless body area networks, IET Communications 10 (1) (2016) 81–90.

[10] A. A. Diaz, B. Celli, J. C. Celedón, Chronic obstructive pulmonary disease in hispanics. a 9-year update, American journal of respiratory and critical care medicine 197 (1) (2018) 15–21.

[11] R. V. M. da Nóbrega, M. B. Rodrigues, P. P. Rebouças Filho, Segmentation and visualization of the lungs in three dimensions using 3d region growing and visualization toolkit in ct examinations of the chest, in: 2017 IEEE 30th International Symposium on Computer-Based Medical Systems (CBMS), IEEE, 2017, pp. 397–402.

[12] A. El-Baz, G. M. Beache, G. Gimel'farb, K. Suzuki, K. Okada, A. Elnakib, A. Soliman, B. Abdollahi, Computer-aided diagnosis systems for lung cancer: challenges and methodologies, International journal of biomedical imaging 2013 (2013).

[13] A. G. Medeiros, D. S. Ferreira, Detecção de agrupamentos de microcalcificações em imagens digitais de mamografias, XV WIM - Workshop de Informática Médica, Recife - PE (2015).

[14] J. H. da Silva Felix, P. C. Cortez, R. C. S. Costa, S. C. B. Fortaleza, et al., Avaliação computacional de enfisema pulmonar em TC: comparação entre um sistema desenvolvido localmente e um sistema de uso livre, Jornal Brasileiro de Pneumologia 35 (9) (2009) 868–876.

[15] S. Avinash, K. Manjunath, S. S. Kumar, An improved image processing analysis for the detection of lung cancer using gabor filters and watershed segmentation technique, in: International Conference on Inventive Computation Technologies (ICICT), Vol. 3, IEEE, 2016, pp. 1–6.

[16] R. Filho, P. C. Cortez, A. C. S. Barros, V. H. C. D. Albuquerque, Novel adaptive balloon active contour method based on internal force for image segmentation–A systematic evaluation on synthetic and real images, Expert Systems with Applications 41 (17) (2014) 7707–7721.

[17] G. Ding, S. Khan, Z. Tang, F. Porikli, Feature mask network for person re-identification, Pattern Recognition Letters (2019).

[18] Y. Yu, K. Zhang, L. Yang, D. Zhang, Fruit detection for strawberry harvesting robot in non-structural environment based on mask-rcnn, Computers and Electronics in Agriculture 163 (2019) 104846.

[19] H.-C. Shin, H. R. Roth, M. Gao, L. Lu, Z. Xu, I. Nogues, J. Yao, D. Mollura, R. M. Summers, Deep convolutional neural networks for computer-aided detection: Cnn architectures, dataset characteristics and transfer learning, IEEE transactions on medical imaging 35 (5) (2016) 1285–1298.

[20] K. He, G. Gkioxari, P. Dollár, R. Girshick, Mask r-cnn, in: Proceedings of the IEEE international conference on computer vision, 2017, pp. 2961–2969.

[21] V. Couteaux, S. Si-Mohamed, O. Nempont, T. Lefevre, A. Popoff, G. Pizaine, N. Villain, I. Bloch, A. Cotten, L. Boussel, Automatic knee meniscus tear detection and orientation classification with mask-rcnn, Diagnostic and interventional imaging 100 (4) (2019) 235–242.

[22] A. G. Medeiros, F. H. Silva, E. F. Ohata, S. A. Peixoto, P. P. R. Filho, An automatic left ventricle segmentation on echocardiogram exams via morphological geodesic active contour with adaptive external energy (2019).

[23] P. P. Rebouças Filho, P. C. Cortez, M. A. Holanda, Modelo de contorno ativo crisp: nova técnica de segmentação dos pulmões em imagens de TC, Revista Brasileira de Engenharia Biomédica 27 (4) (2011) 259–72.

[24] P. P. Rebouças Filho, P. C. Cortez, J. H. d. S. Felix, T. d. S. Cavalcante, M. A. Holanda, Modelo de Contorno Ativo Crisp Adaptativo 2D aplicado na segmentação dos pulmões em imagens de TC do tórax de voluntários sadios e pacientes com enfisema pulmonar, Revista Brasileira de Engenharia Biomédica 29 (2013) 363 – 376.

[25] A. G. Medeiros, S. A. Peixoto, A. C. S. Barros, V. H. C. de Albuquerque, P. P. Rebouças Filho, Uma nova abordagem para a segmentação de pulmões utilizando o método de contorno ativo não paramétrico optimum path snakes em imagens de tomografia computadorizada.

[26] M. Kass, A. Witkin, D. Terzopoulos, Snakes: Active contour models, International journal of computer vision 1 (4) (1988) 321–331.

[27] A. G. Medeiros, M. T. Guimarães, S. A. Peixoto, L. d. O. Santos, A. C. da Silva Barros, E. d. S. Rebouças, V. H. C. de Albuquerque, P. P. Rebouças Filho, A new fast morphological geodesic active contour method for lung ct image segmentation, Measurement 148 (2019) 106687.

[28] C. Xu, J. L. Prince, Snakes, shapes, and gradient vector flow, IEEE Transactions on image processing 7 (3) (1998) 359–369.

[29] B. Li, S. T. Acton, Vector field convolution for image segmentation using snakes, in: 2006 International Conference on Image Processing, IEEE, 2006, pp. 1637–1640.

[30] P. P. Rebouças Filho, P. C. Cortez, J. H. d. S. Félix, T. d. S. Cavalcante, M. A. Holanda, Adaptive 2d crisp active contour model applied to lung segmentation in ct images of the thorax of healthy volunteers and patients with pulmonary emphysema, Revista Brasileira de Engenharia Biomédica 29 (4) (2013) 363–376.

[31] A. C. da Silva Barros, Optimum path snakes: Novo método de contornos ativos adaptativo e não-paramétrico, Ph.D. thesis, Universidade de Fortaleza, Fortaleza, CE (2016).

[32] J. H. d. S. Felix, P. C. Cortez, A. R. Alexandria, P. P. Rebouças Filho, T. Cavalcante, M. A. Holanda, Novo método de contornos ativo baseado na transforma de hilbert radial, in: V Latin American Congress on Biomedical Engineering CLAIB 2011 May 16-21, 2011, Habana, Cuba, Springer, 2013, pp. 1051–1053.

[33] S. Osher, J. A. Sethian, Fronts propagating with curvature-dependent speed: algorithms based on hamilton-jacobi formulations, Journal of computational physics 79 (1) (1988) 12–49.

[34] V. Caselles, R. Kimmel, G. Sapiro, Geodesic active contours, International journal of computer vision 22 (1) (1997) 61–79.

[35] P. Marquez-Neila, L. Baumela, L. Alvarez, A morphological approach to curvature-based evolution of curves and surfaces, IEEE Transactions on Pattern Analysis and Machine Intelligence 36 (1) (2014) 2–17.

[36] R. Girshick, J. Donahue, T. Darrell, J. Malik, Rich feature hierarchies for accurate object detection and semantic segmentation, in: Proceedings of the IEEE conference on computer vision and pattern recognition, 2014, pp. 580–587.

[37] R. Girshick, Fast r-cnn, in: Proceedings of the IEEE international conference on computer vision, 2015, pp. 1440–1448.

[38] S. Ren, K. He, R. Girshick, J. Sun, Faster r-cnn: Towards real-time object detection with region proposal networks, in: Advances in neural information processing systems, 2015, pp. 91–99.

[39] S. A. Peixoto, P. P. Rebouças Filho, N. A. Kumar, V. H. C. de Albuquerque, Automatic classification of pulmonary diseases using a structural co-occurrence matrix, Neural Computing and Applications (2018) 1–11.

[40] E. S. . O. S. A. F. . B. A. M. . R. F. P. P. ALVES, S. S. A. REBOUçAS, Lung diseases classification by analysis of lung tissue densities, IEEE Latin America Transactions (2018).

[41] P. P. R. Filho, E. de S. Rebouças, L. B. Marinho, R. M. Sarmento, J. M. R. Tavares, V. H. C. de Albuquerque, Analysis of human tissue densities: A new approach to extract features from medical images, Pattern Recognition Letters 94 (2017) 211 – 218. doi:https://doi.org/10.1016/j.patrec.2017.02.005.

[42] A. G. Medeiros, S. A. Peixoto, A. C. S. Barros, V. H. C. de Albuquerque, P. P. Rebouças Filho, Uma nova abordagem para a segmentação de pulmões utilizando o método de contorno ativo não paramétrico optimum path snakes em imagens de tomografia computadorizada, in: Anais do XVII Workshop de Informática Médica, SBC, 2017.

[43] T. Fawcett, An introduction to roc analysis, Pattern recognition letters 27 (8) (2006) 861–874.

[44] M. Sokolova, G. Lapalme, A systematic analysis of performance measures for classification tasks, Information processing & management 45 (4) (2009) 427–437.

[45] K. Van Deemter, A. Gatt, Beyond dice: measuring the quality of a referring expression, in: Proc. of the workshop preCogSci-09, 2009.

[46] B. W. Matthews, Comparison of the predicted and observed secondary structure of t4 phage lysozyme, Biochimica et Biophysica Acta (BBA)-Protein Structure 405 (2) (1975) 442–451.

[47] P. Jaccard, Étude comparative de la distribution florale dans une portion des alpes et des jura, Bull Soc Vaudoise Sci Nat 37 (1901) 547–579.

[48] J. Henrikson, Completeness and total boundedness of the hausdorff metric, MIT Undergraduate Journal of Mathematics 1 (1999) 69–80.

[49] A. M. Reza, Realization of the contrast limited adaptive histogram equalization (clahe) for real-time image enhancement, Journal of VLSI signal processing systems for signal, image and video technology 38 (1) (2004) 35–44.

[50] M. Sepasian, W. Balachandran, C. Mares, Image enhancement for fingerprint minutiae-based algorithms using clahe, standard deviation analysis and sliding neighborhood, in: Proceedings of the World congress on Engineering and Computer Science, 2008, pp. 22–24.

[51] B. Kurt, V. V. Nabiyev, K. Turhan, Medical images enhancement by using anisotropic filter and clahe, in: 2012 International Symposium on Innovations in Intelligent Systems and Applications, IEEE, 2012, pp. 1–4.

[52] B. Singh, S. Patel, Efficient medical image enhancement using clahe enhancement and wavelet fusion, International Journal of Computer Applications 167 (5) (2017) 0975–8887.

[53] S. Sahu, A. K. Singh, S. Ghrera, M. Elhoseny, et al., An approach for de-noising and contrast enhancement of retinal fundus image using clahe, Optics & Laser Technology 110 (2019) 87–98.

[54] P. P. Reboucas Filho, E. d. S. Reboucas, L. B. Marinho, R. M. Sarmento, J. M. R. Tavares, V. H. C. de Albuquerque, Analysis of human tissue densities: A new approach to extract features from medical images, Pattern Recognition Letters 94 (2017) 211–218.

978-1-7281-6926-2/20/$31.00 ©2020 IEEE